Geomechanics and Engineering, *Vol. 24, No. 5 (2021) 419-430*
DOI: https://doi.org/10.12989/gae.2021.24.5.419

Effects of dry density and water content on compressibility and shear strength of loess

Yexia Guo[a], Wankui Ni* and Haisong Liu[b]

School of Geology Engineering and Geomatics, Chang'an University, 710064 Xi'an, Shannxi Province, China

(Received December 2, 2020, Revised January 29, 2021, Accepted February 16, 2021)

Abstract. Investigation on the compressibility and shear strength of compacted loess is of great importance for the design and operation of engineering infrastructures in filling area. In this study, the mechanical behaviors of Yan'an compacted loess are investigated at various dry densities and water contents by conducting one dimensional compression and direct shear tests. And the elastic compressibility, plastic compressibility, yield stress and strength are obtained from the experiments. Results show that when water content increases, plastic compressibility parameter increases, but yield stress decreases. However, the increase of dry density leads to a decrease in plastic compressibility parameter but an increase in yield stress. In addition, elastic compressibility parameter is found to be a constant which is irrelevant to water content and dry density. As for strength, cohesion and internal friction angle is directly proportional to dry density, but inversely proportional to water content. Moreover, the mercury intrusion porosimetry (MIP) and scanning electron microscope (SEM) tests were also performed to observe the pore size distribution and microstructure of the specimens. Finally, by using results of MIP and SEM tests, the compressibility and strength behaviours of Yan'an compacted loess are explained from the perspective of pore-size distribution and microstructure.

Keywords: water content; dry density; compression parameters; shear strength; microstructure

1. Introduction

With the implementation of Chinese national programs like the Silk Road Economic Belt, land scarcity has seriously restricted the local development in Northwestern China including Yan'an city. In order to create more space for construction, local Yan'an loess has been an alternative filling material by cutting hills and filling valleys (Hu *et al*. 2018). During and after the filling projects, loess is usually compacted to some extent, built as foundations, pathways, rivers and so on (Kim *et al*. 2013, Parviz *et al*. 2020). Since water content and void ratio varies of filling loess soils inevitably which sharply influence the basic mechanical characteristics of local loess, a deep understanding of the compressibility and shear strength of Yan'an loess in the filling area is crucially basic before construction.

The mechanical behaviour of loess has been widely investigated in the previous literatures (Derbyshire *et al.* 1988, Haeri *et al.* 2016, Yates *et al.* 2018, Wang *et al.* (2019). It was found that the compression behavior can be influenced by many factors, such as void ratio, degree of saturation, structure index, matric suction, *etc*. They pointed out that the water content and void ratio could affect compression and collapse behaviors of loess to a great extent. And the initial structural would result in a larger compressive yield stress in natural loess. Several researchers (Cui and Delage. 1996, Estabragh *et al.* 2015) investigated the influence of water content on compressibility parameters during consolidation test in the framework of unsaturated soil mechanics. They showed that the pre-consolidated pressure p_0 would increase and the slope of normal compression line in v-lnp' plane would decrease with water content decreasing. For low-plasticity loess soils, it has been commonly observed that elastic compressibility parameter (κ) is slightly dependent on the water content (Alshihabi *et al.* 2002, Cui and Delage 1996, Cuisinier and Masrour 2005). As for shear strength, some researchers believed that reduction of loess's shear strength was due to the decrease in matric suction upon wetting (Fredlund and Rahardjo 1993, Muñoz-Castelblanco *et al.* 2012, Wen *et al.* 2014). Others attributed loss of loess's strength to the weakening of inter-particle bonds provided by clay and carbonates (Rogers *et al.* 1994; Dijkstra *et al.* 1995; Kruse Gerard *et al.* 2007). The degree of structure on its strength behavior remains to be an active subject to consider. Assallay *et al.* (1997) analyzed the effect of the degree of structure on mechanical strength of loess, the test results indicated that the undisturbed loess specimens had larger effective cohesion but less internal friction angles compared to the corresponding remolded ones. In addition, the microstructure of soil plays a decisive role in all aspects of soil properties, and the mechanical properties of soil can be understood as the macroscopic performance of

*Corresponding author, Professor
E-mail: niwankui123@163.com
[a]Ph.D.
E-mail: guoyx0911@163.com
[b]Professor
E-mail: 2016026028@chd.edu.cn

ISSN: 2005-307X (Print), 2092-6219 (Online)

Fig. 1 Field exploration well sampling

Table 1 Physical parameters of tested loess

Properties	w_n (%)	LL (%)	PI	G_s	Clay (%)	Silt (%)	Sand (%)	MDD (Mg/m^3)	OMC (%)
Values	28.1	25.5	9	2.70	15	76	9	1.78	14.0

microstructure. Therefore, in order to further understand the engineering properties of soil, it is necessary to further study the microstructure of soil (Monroy *et al.* 2010, Casini *et al.* 2012, Chen *et al*. 2019, Niu *et al*. 2020). Thus, investigating the microstructure in different initial dry density and water content and the compressibility and strength behaviors in different initial dry density and water content, which can lead to a better understanding of the compressibility and strength behaviors of loess from the perspective of pore-size distribution and microstructure.

In this study, one-dimensional compression and direct shear tests are performed on Yan'an compacted loess with different dry densities and water contents. The effects of dry density and water content on the compressibility parameters are analyzed in terms of elastic and plastic compressibility parameters, as well as the yield stress. Moreover, the shear strength is studied in the framework of Mohr-Coulomb theory. Furthermore, scanning electron microscope (SEM) and mercury intrusion porosimetry (MIP) tests are also conducted, studying the pore size distribution and microstructure of the specimens with different density and water content, and explaining the effect of water content and dry density on the mechanical behaviour from the microstructural point of view.

2. Materials and methods

2.1 Material and specimens preparation

The tested loess soil samples are collected from a filling site in Yan'an city, in northwestern Loess Plateau of Shannxi Province, China (Fig. 1). They are sealed in plastic tubes to prevent water evaporation. Table 1 shows the basic physical properties of the tested loess.

To investigate the effect of water content and dry density on the compression and strength behavior of the compacted loess soils, four kinds of initial water content (w_i) are chosen in this study. For each case of w_i, five groups of initial dry density (di) are designed. The testing program is shown in Table. 2.

To prepare the test specimens, the natural loess soils are firstly air-dried, and then sieved using a 2 mm sieve. In accordance with the test program (Table 2), a predetermined mass of distilled water is added to the air-dried loess and thoroughly mixed using a paddle mixer. The soil mixtures are then placed in plastic bags to avoid any changes in water content, and cured at a temperature of 20 °C (relative humidity of 95%) for 48 h. After curing, the predetermined wetted mixtures are weighed and placed into an oedometer cell (20 mm in height, 61.8 mm in diameter), respectively. In order to reduce the internal force between the inner wall and the specimen, the inner wall of the cell is lubricated with silicon grease in advance. Thereafter, compaction is achieved via a piston at a rate of 0.4 mm/min. When the targeted dry density ρ_d is obtained, the compaction would stop and the same compaction load would maintain for 1 h. In this study, for each w_i, five specimens of different dry densities (ρ_d =1.55, 1.60, 1.65, 1.70, 1.75 Mg/m^3) are compacted.

2.2 Oedometer compression and direct shear tests

In oedometer tests, the soil specimens are firstly placed on WG triple high pressure oedometer apparatuses, then subjected to an increasing vertical stress of 25, 50, 100, 200, 400, 800, 1600 and 3200 kPa step by step without contacting with water in order to eliminate the swelling/collapse.

The direct shear test is done under unconsolidated and undrained condition. Firstly, the prepared test specimens with 20 mm height and 61.8 mm diameter are installed in ZJ type quadruple direct shear apparatus and both the top and bottom of specimens are covered with waterproof paper to prevent the initial water content drained, then subjected to certain vertical stresses (50, 100, 200, 400 kPa), followed

Table 2 Testing program in this study

Label	Specimen Nunber	v_i (cm^3)	m_s (g)	m_w (g)	w_i (%)	ρ_{di} (Mg/m^3)	e_i
A	A-1	60	92.87	5.57	6	1.55	0.744
	A-2	60	95.69	5.74	6	1.60	0.693
	A-3	60	98.75	5.93	6	1.65	0.640
	A-4	60	102.10	6.13	6	1.70	0.586
	A-5	60	104.80	6.29	6	1.75	0.546
B	B-1	60	92.87	9.29	10	1.55	0.744
	B-2	60	95.93	9.59	10	1.60	0.689
	B-3	60	99.11	9.91	10	1.65	0.634
	B-4	60	101.86	10.19	10	1.70	0.590
	B-5	60	104.74	10.47	10	1.75	0.546
C	C-1	60	92.87	13.00	14	1.55	0.744
	C-2	60	95.99	13.44	14	1.60	0.688
	C-3	60	98.99	13.86	14	1.65	0.636
	C-4	60	101.98	14.28	14	1.70	0.588
	C-5	60	104.98	14.70	14	1.75	0.543
D	D-1	60	93.35	16.80	18	1.55	0.735
	D-2	60	95.87	17.26	18	1.60	0.690
	D-3	60	99.05	17.83	18	1.65	0.635
	D-4	60	101.92	18.35	18	1.70	0.589
	D-5	60	105.10	18.92	18	1.75	0.541

by the horizontal shear force are immediately applied. During the shearing process, a constant shear rate of 0.08 mm/min are maintained to a maximum horizontal displacement of 5 mm for all shearing tests. The shear damaged finished within 3-5 min, hence, the pore water pressure remains unchanged during the direct shear test.

2.3 SEM and MIP tests

In order to evaluate the effect of water content and dry density on mechanical behavior of loess from microstructural point of view, a series of SEM and MIP tests are conducted.

For the SEM tests, specimens with dry density of 1.70 Mg/m^3 but different initial water contents of 10%, 14% and 18%, as well as specimens with initial water content of w_i=14% but different dry densities of 1.60, 1.70 and 1.75 Mg/m^3 are examined using SEM. Three blocks with dimensions of 10 mm×10 mm×20 mm are firstly taken and immersed in liquid nitrogen for instantly freezing. Then, the frozen specimens are immediately transferred to a vacuum chamber for freeze drying for 24 h (Penumadu and Dean 2000). Finally, these prepared specimens are peeled to expose a fresh surface and coated with a 200-300 Å thick gold layer to provide electrical conductivity on surfaces.

For the MIP tests, a small piece of specimen is freeze-dried following the proposed by Delage *et al*. (2006). An autopore IV9500 MIP is used. This machine has two systems: a low-pressure system with a working capacity from 3.6 kPa to 200 kPa and a high-pressure system with a working capacity from 0.2 MPa to 210 MPa. These pressures by two systems define maximum and minimum entrance diameters of 350-0.006 μm. The MIP tests are performed on specimens with dry density of 1.70 Mg/m^3 and water contents of 6%, 10%, 14% and 18%, as well as water content of 14% and dry densities of 1.60, 1.70 and 1.75 Mg/m^3.

3. Results

3.1 Compression behavior

Fig. 2 shows the relationship between void ratio e and vertical stress σ_v of the specimens with various dry densities at different initial water content. It can be observed that these compression curves are characterized by an initial linear part with low compressibility (that could be considered as the pseudo-elastic domain) followed by a second part with higher compressibility (that could be considered as the plastic domain).

By approximating the curve of ratio e vs vertical stress σ_v with two straight lines, the slopes of the two straight lines are the elastic and the plastic compressibility parameters (κ and λ) respectively, the stress at the intersection point of the two straight lines is the yield stress σ'_y (corresponding to the common pre-consolidation pressure σ'_p) (see Fig. 3) (Lloret *et al.* 2003), and these values are replotted in Fig. 4 in terms of compressibility parameters (Fig. 4(a)) and yield stress (Fig. 4(b)) versus dry density at different water content. It could be observed from Fig. 4(a) that the plastic compressibility parameter λ decreases with the increase of

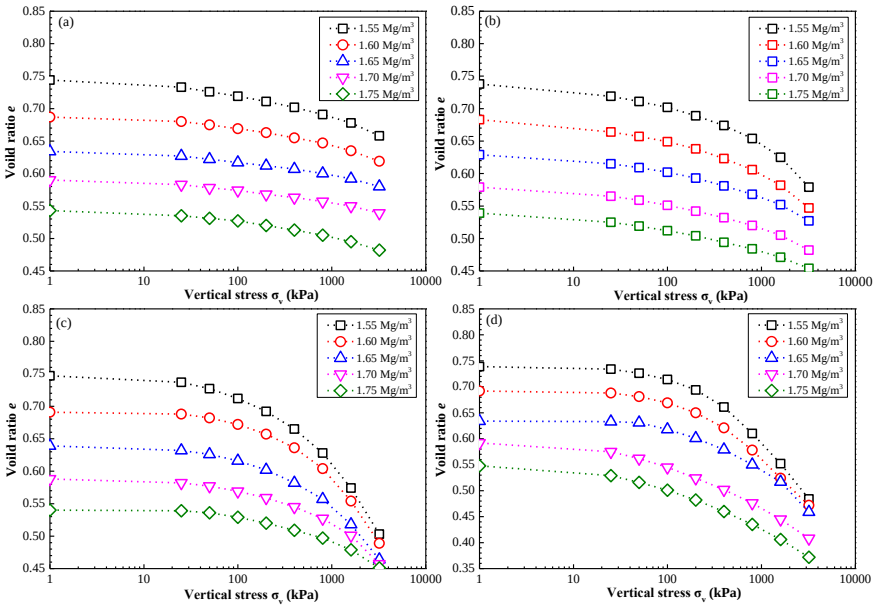

Fig. 2 Compression curves of compacted loess with different dry densities at different initial water content: (a) w_i=6%, (b) w_i=10%, (c) w_i=14% and (d) w_i=18%

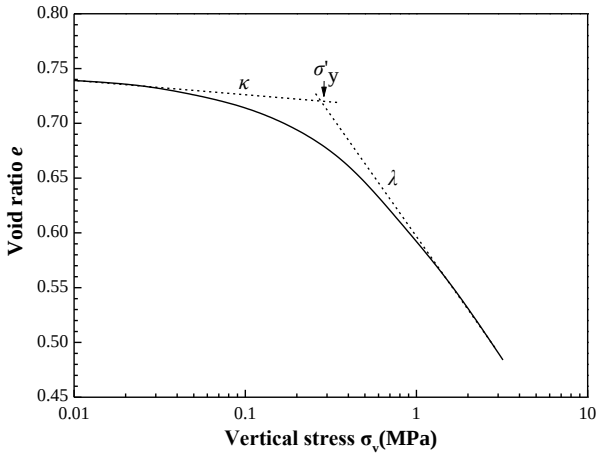

Fig. 3 Schematic diagram of determination of compressibility parameters κ, λ and σ'_y

dry density ρ_d and increases with the increase of initial water content w_i. For those with high initial water contents (larger than 10%), the plastic compressibility parameter λ decreases significantly with the increasing dry density, and the maximum and minimum values of λ are 0.147 and 0.060, respectively. By contrast, for the specimens with the lower initial water content (6%), plastic compressibility parameter λ is reduced significantly with the increase of the dry density, with the maximum and minimum values of 0.029 and 0.014, respectively. This phenomenon indicates that both the initial dry density and initial water content have significant effects on the plastic compressibility parameter λ, but negligible effects on the elastic compressibility parameter κ, so the elastic compressibility parameter κ can be determined by the average value of all the test values, and it is typically calibrated as 0.008. This is consistent with the results reported by Zhang *et al*. (2016). Results in Fig. 4(b) show that dry density and initial water content have a significant influence on the yield stress σ'_y, and the yield stress σ'_y linearly increases with the increase of dry density ρ_d. Moreover, the higher the initial water content w_i, the lower the yield stress σ'_y.

3.2 Shear strength

According to Mohr-Coulomb's law, the fixed shear plane of specimen is directly applied the horizontal shear force when the specimen is subject to different normal pressures of 50, 100, 200, 400 kPa, respectively, then, the shear stress obtained when the fixed shear plane failure is the shear strength q. Fig. 5 shows the variation of shear strength of compacted loess specimens with dry densities and water contents under normal pressures conditions (p=50, 100, 200, 400 kPa). It appears from Fig. 5 that the shear strength increases with increasing dry density, but decreases with increasing initial water content. Moreover, the effect of dry density on the shear strength depends on the initial water content. For low water content (e.g., 6%),

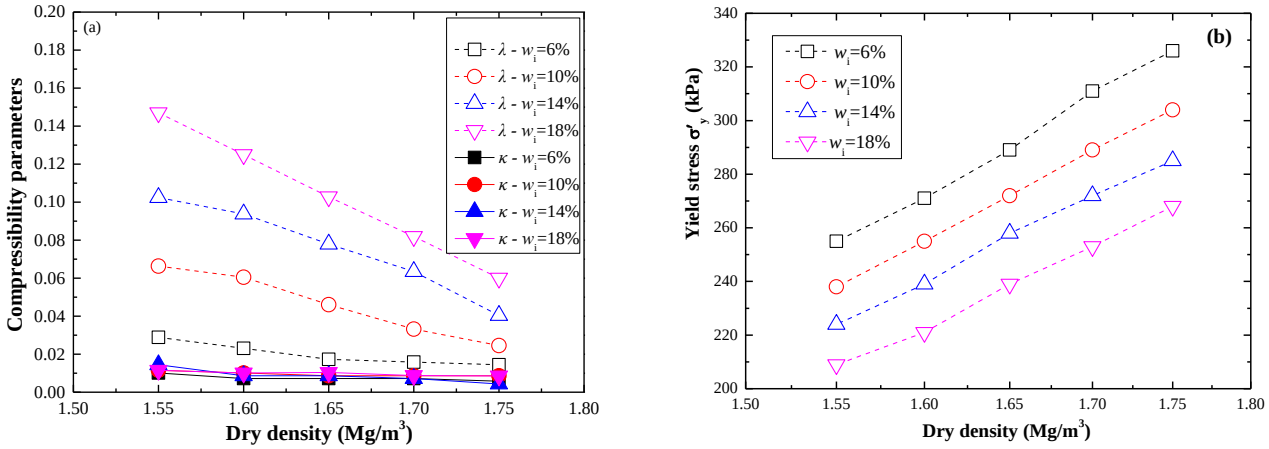

Fig. 4 Compressibility parameters κ, λ and σ'_y of specimens with various dry densities under different initial water content: (a) κ and λ and (b) σ'_y

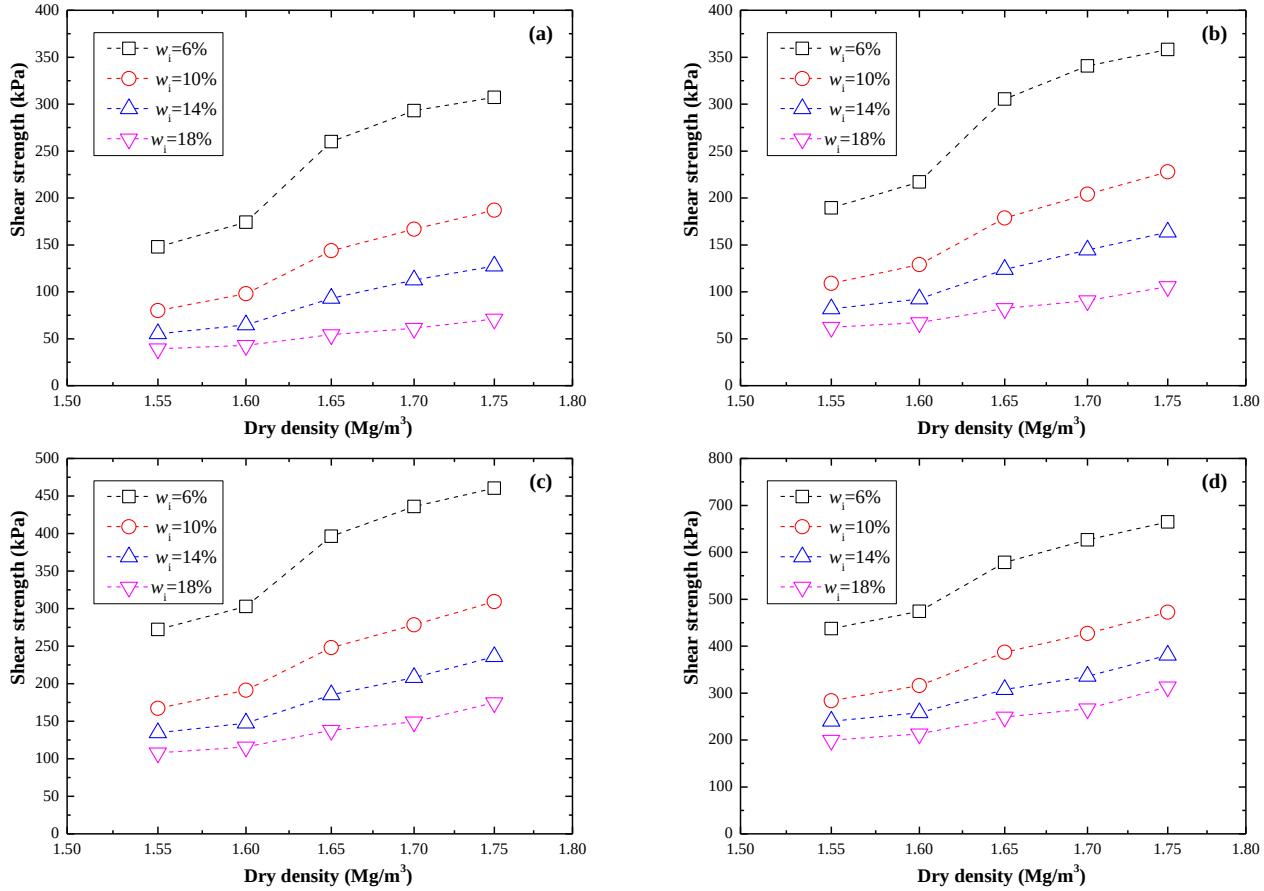

Fig. 5 Curves of peak shear strength of specimens versus different dry densities and initial water content under different normal pressure: (a) p=50 kPa, (b) p=100 kPa, (c) p=200 kPa and (d) p=400 kPa

the shear strength significantly increases from 148 to 307 kPa as the dry density increases from 1.55 to 1.75 Mg/m^3. By contrast, for higher water content (e.g., 18%), the effect of dry density becomes negligible. This phenomenon indicates that the shear strength is weakened with increasing dry density, especially for specimens with low w_i.

Fig. 6 presents the representative peak shear strength envelopes of these specimens with different dry densities at different initial water contents. It is found that the peak shear strength increases with the increase of normal pressure and dry density, but decreases with the increase of water content.

In Fig. 6, the intercept of the peak shear strength envelope to the Y-axis and the angle between the shear strength envelope and the X-axis are cohesion c and internal friction angles φ of shear strength parameters, respectively.

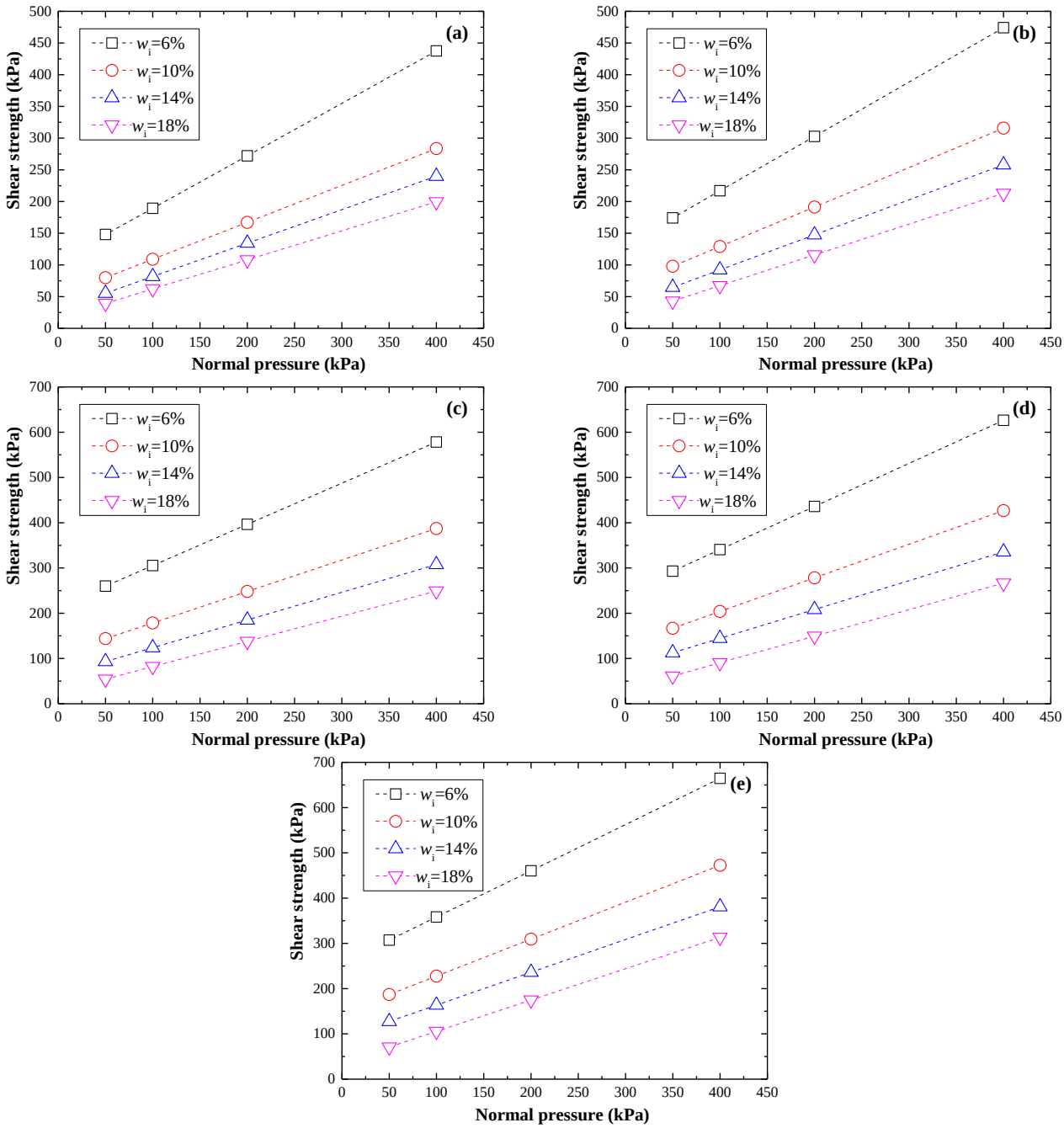

Fig. 6 Peak shear strength envelopes of the specimens: (a) ρ_d=1.55 Mg/m^3, (b) ρ_d=1.60 Mg/m^3, (c) ρ_d=1.65 Mg/m^3, (d) ρ_d=1.70 Mg/m^3 and (e) ρ_d=1.75 Mg/m^3

The shear strength parameters (cohesion c and internal friction angles φ) of these specimens are obtained from the shear strength envelopes, as shown in Fig. 7 and Table 3. It can be observed from Fig. 7 that the cohesion (c) and the internal friction angles (φ) of compacted loess specimens exhibit a decreasing tendency with the increase of initial water contents but an increasing tendency with the increase of dry densities (Fig. 7). Note that, for the specimens with water content of 6%, the cohesion is decreased from 256 to 107 kPa as the dry density is decreased from 1.75 to 1.55 Mg/m^3. However, when the water content is 18%, the variation of the cohesion is less important. It varies from 36 to 16 kPa as dry density decreases from 1.75 to 1.55 Mg/m^3, indicating the dry density has insignificant effects on shear strength under the case of compacted loess with high water content. In terms of reduction degree for the specimens with the same dry density, the reduction degree in cohesion c with the increasing water content is greater than that in internal friction angles φ, and water content has less influences on the internal friction angles φ when the dry density is exceeded 1.70 Mg/m^3. This indicates that cohesion c of compacted loess is more sensitive to water content than internal friction angles φ, and the reduction of cohesion c is mainly contributed to the decrease of shear strength of remolded loess upon wetting.

Table 3 Shear strength parameters of the compacted specimens with different dry density and water content

ρ_d (Mg/m^3)	Strength parameter	Water content (%)			
		6	10	14	18
1.55	c (kPa)	106.6	50.8	29	16.4
	φ (°)	39.6	30.2	27.8	24.6
1.60	c (kPa)	131.3	66.8	37.1	18.7
	φ (°)	40.6	31.9	28.9	25.9
1.65	c (kPa)	214.4	109.1	62.5	26.5
	φ (°)	42.3	34.8	31.5	29.1
1.70	c (kPa)	245.4	129.7	80.8	31.9
	φ (°)	43.6	36.6	32.5	30.4
1.75	c (kPa)	256.1	146.2	91.3	36.3
	φ (°)	45.6	39.2	35.9	34.7

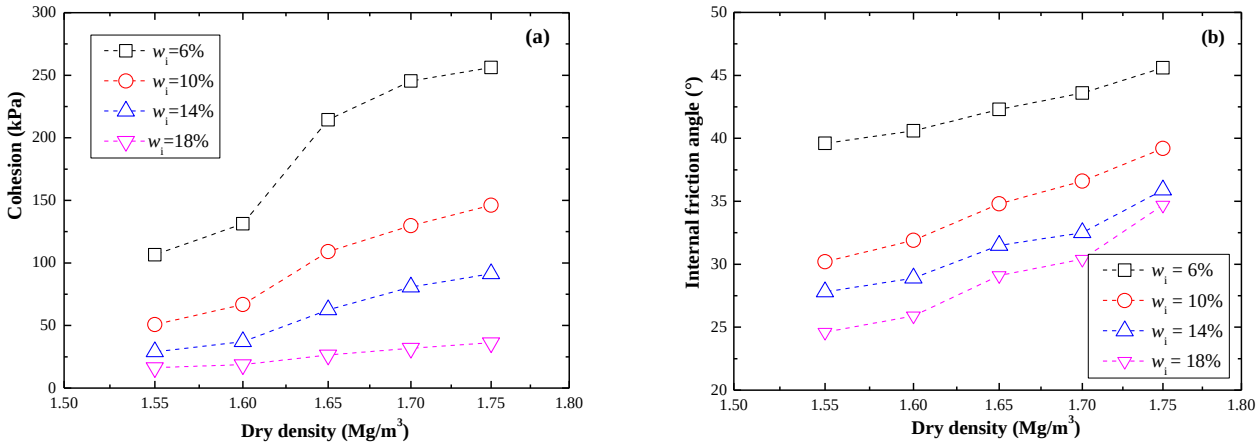

(a) c *vs* ρ_d (b) φ *vs* ρ_d

Fig. 7 Relationship between shear strength parameters and water content of the compacted specimens

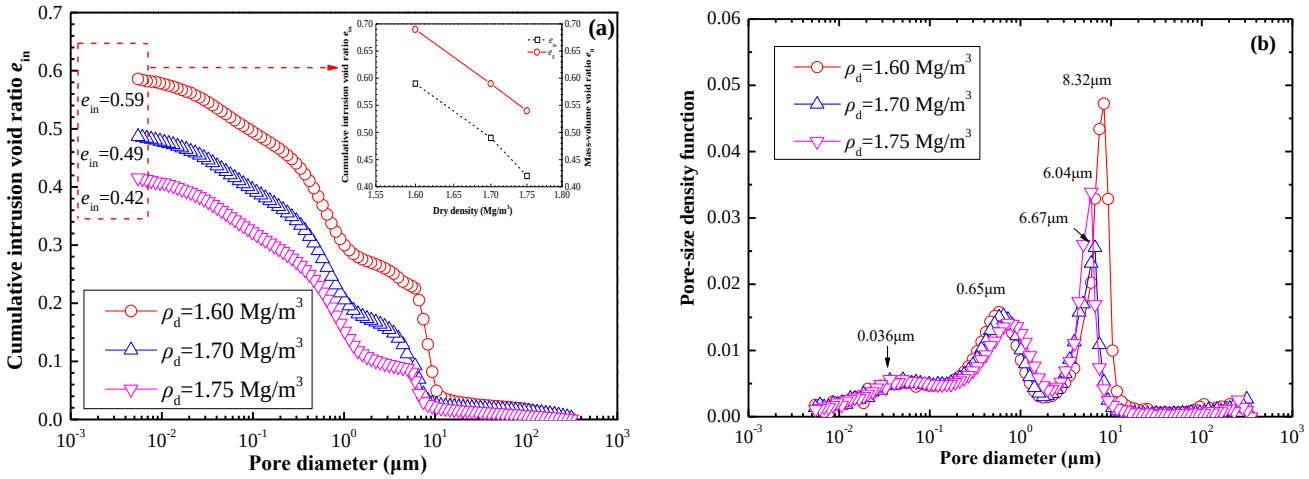

(a) Cumulative pore volume (b) Pore-size density

Fig. 8 MIP results of the compacted loess specimens of w_i=14% at different dry densities

3.3 Microstructure feature

Fig. 8 presents the pore size distributions of specimens of water content w_i=14% at dry densities of 1.60, 1.70 and 1.75 Mg/m^3 in terms of cumulative pore volume and pore-size density function. The cumulative pore volume curves in Fig. 8(a) indicates that the intrusion porosity of specimens decreases with the increase of dry density, and the cumulative intrusion void ratio e_{in} are 0.59, 0.49, 0.42. They can be obtained by directly multiplying the

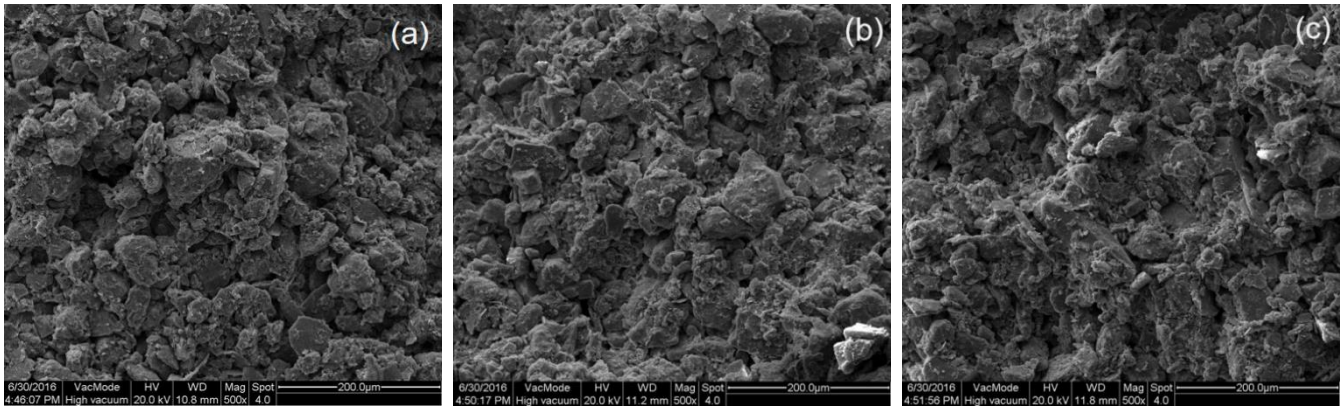

Fig. 9 SEM results of compacted loess specimens of w_i=14% with different dry densities: (a) 1.60 Mg/m^3, (b) 1.70 Mg/m^3 and (c) 1.75 Mg/m^3

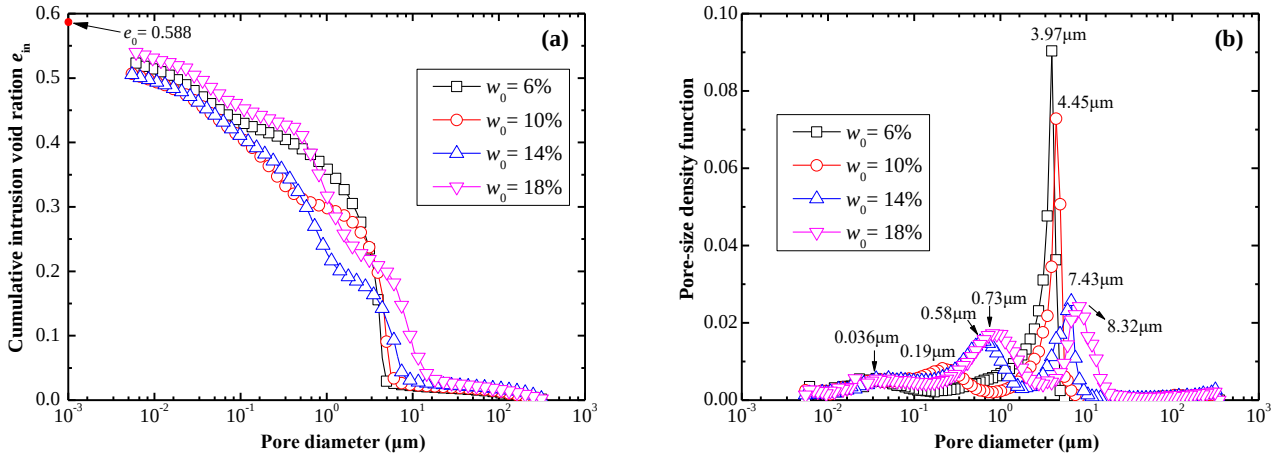

(a) Cumulative pore volume (b) Pore-size density functions

Fig. 10 MIP results of the compacted loess specimens of ρ_d=1.70 Mg/m^3 at different water content

cumulative pore volume data by specific gravity of loess (2.7 Mg/m^3), the variation trend of MIP test result is smaller than the void ratio e_0 obtained according to the mass-volume relations, which are 0.69, 0.59 and 0.54 corresponding to dry densities of 1.60, 1.70 and 1.75 Mg/m^3. This is due to the limited pore size (0.006-360 μm) that could be detected by the porosimetry employed (Delage *et al.* 2006, Wang *et al.* 2019). With the increase of dry density, the compactness degree of specimen is increasing, which could lead to more larger pores transforming into small pores and increase more enclose pores and constricted pores which couldn't been detected and intruded, so the difference between intrusion void ratio e_{in} and mass-volume void ratio e_0 increase slight with the dry density (e_0-e_{in}).

Fig. 8(b) shows a tri-modal density function curves for specimens with dry densities of 1.60, 1.70 and 1.75 Mg/m^3. Four pore families are defined to provide qualitative analysis of the pore size distribution: inaccessible pores (< 0.006 μm and >350 μm), small pores (0.006-0.1 μm), medium pores (0.1-2 μm) and large pores (2-350 μm) (Collins and McGown 1974, Romero *et al.* 2011, Ng *et al.* 2016). The dominated peaks of small pores and medium pores are found to be similar for specimens with different dry density, being equal to 0.036 μm and 0.65 μm, respectively. However, the dominated peaks of large pores decrease with the increase of dry density: 8.32, 6.67 and 6.04 μm for the specimens with dry densities of 1.60, 1.70 and 1.75 Mg/m^3, respectively. The results identified here suggest that the dry density has significant effect on the large pores, and insignificant effect on the small and medium pores.

Fig. 9 summarizes the SEM pictures of compacted loess specimens of various dry densities, which are compacted using static compaction method with an increasing compaction energy. It is equivalent to consolidate the compacted loess under various stress levels (Wang *et al.* 2019), the increasing compactness has a significant influence on the compacted loess structure. Fig. 9 shows that the aggregates become deformable and breakable enough to give a massive and dense matrix microstructure with the increase of compaction energy, the compacted loess fabric transforms from an aggregate (silt-clay and clay aggregates) type into a matrix type in response to the increase in dry density (or compaction energy). Hence, it can be observed in Fig. 9(b) and 9(c) that the increase in dry density of compacted loess resulting in a smaller size and closer arrangement of aggregates and smaller pores. In addition, the morphology of the aggregate could be changed by increasing compaction energy to achieve a closer arrangement of the aggregate (see Fig. 9(b) and 9(c)) (Chen

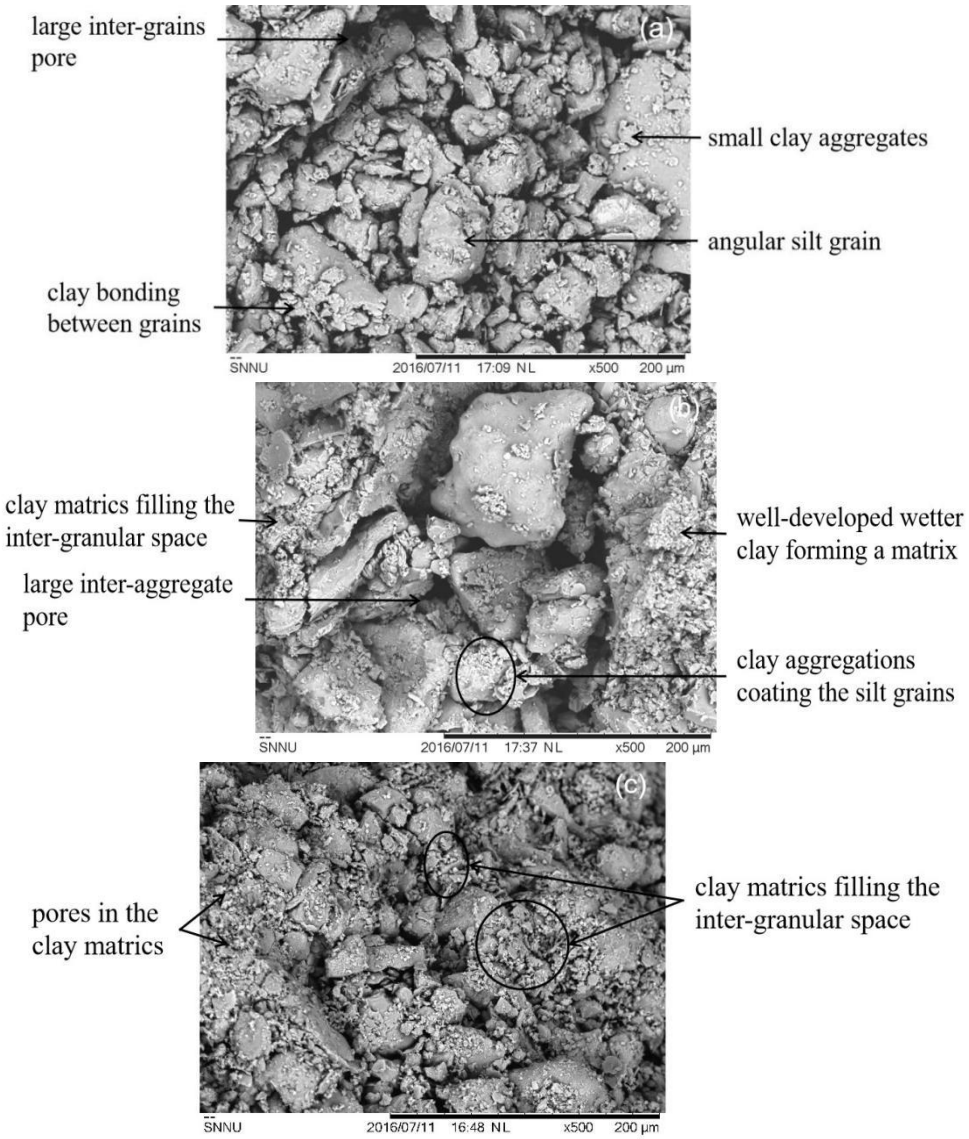

Fig. 11 SEM results of compacted specimens of dry density 1.70 Mg/m^3: (a) w_i= 10%, (b) w_i=14% and (c) w_i=18%

et al. 2019).

Fig. 10 presents the MIP results of pore size distribution of specimens of dry density 1.70 Mg/m^3 at water contents of 6%, 10%, 14% and 18% in terms of cumulative intrusion void ratio e_{in} (Fig. 10(a)) and pore-size density function (Fig. 10(b)). It can be observed from Fig. 10(a) that all the intruded e_{in} is smaller than the soil void ratio measured in the lab e_0 and the void ratio e_0 is about 0.585 for each specimen. Moreover, the intruded e_{in} of all the specimens is unequal. This difference is due to the internal structure variation of specimens at various water content obtained in a compression machine, and to the size difference between the compacted specimens and the millimetre-size specimens used for PSD measurements (Wang *et al.* 2019).

Fig. 10(b) shows the curves of pore-size density function of all specimens, it can be seen that: i) the dominated peak of small pores (0.006-0.1 μm) is found to be similar at different initial water content, equal to 0.036 μm; ii) for water content of 6%, the function curve exhibits bimodal porosity, the dominated peaks of small pores and large pores are 0.036 μm and 3.97 μm, respectively; iii) with the increase of water contents, the dominated peak of large pores increased from 3.97 μm (water content of 6%) to 4.45 μm, 7.43 μm and 8.32 μm for water contents of 10%, 14% and 18%, respectively, accompanied by the creation of a new medium pore family, with the dominated peaks of 0.19 μm, 0.58 μm and 0.73 μm for water contents of 10%, 14% and 18%; iv) the dominated peak of small pores kept unchanged.

Fig. 11 shows the SEM pictures of the dry, OMC and wet compacted specimens, i.e., water content of 10%, 14%, 18%, respectively. Fig. 11a of dry specimen (w_i=10%) clearly shows a dominant proportion of angular silt grains with diameters of several tens of micrometers. The figure also shows the clayey fraction is not well developed compared to the wet specimen (Fig. 11(c)). Clays are seen to coat the angular silt grains either in the form of small sized visible clay aggregates or in the form of coatings of very small sized particles to link the silt grains together. Whereas most grains are quite clean, few grains are coated clay aggregates.

The Fig. 11(b) of the OMC specimen (w_i=14%) shows

the previously observed aggregates and clean grains on the dry side are less visible, some clay structure appearing more massive in a clay matrix similar to that found on the wet side, and some coating clayey fractions similar to that found on the dry side. It also can be observed part of the large pores are filled with clayey platelets and transform the medium pores.

The Fig. 11(c) of the wet specimen (w_i=18%) shows a quite different micrograph than that of the dry specimen, despite that the dry density are identical (ρ_d=1.70 Mg/m^3), the silt grains of a few tens of micrometres and small sized aggregates do not stand out. On the wet side, due to hydration, for the same clay content, the clay volume is much large and a structure of well-developed wetter clay forming a matric that envelops the silt grains and fills the inter-granular space. Therefore, in this case, it can be observed that the whole picture is more veiled by a coating of clayey platelets, which are not clearly apparent in the Fig. 11(a), 11(b); largest pores found in the dry specimen are also no longer evident, and a new population of medium pores in porosimetry of Fig. 10(c) is that of the clay matrix pores.

SEM observations of Fig. 11 help to interpret the PSD curve of Fig. 10 in more details. The large inter-grains/aggregates pore and intra-aggregate pore that observed in Fig. 11 belongs to the large pore family and small pore family evidenced by the PSD curve of Fig. 10(b), respectively. As the water content increase, the volume of the silt-clay aggregate becomes larger (Fig. 11), hence the peak value of large pore increases with the increase of water content. Meanwhile, with increasing water content, the structure of the wet clay is fully developed and forms a matrix to fill the intergranular space, then a new pore family is created which corresponding to the medium pore family in Fig. 10 and the number of large pores in wet specimen decreases.

4. Discussion

4.1 Influences of dry density and initial water content on the compressibility parameters (κ, λ and σ'$_y$)

As shown in Fig. 2, when the vertical stress σ_v is smaller than the yield stress σ'_y, the variation of e is pretty small and the compressibility parameter κ, characterizing the variation rate, almost remains constant. Previous studies on reconstituted soils also identify the same variation trend (Alshihabi *et al.* 2002, Cui and Delage 1996, Cuisinier and Masrouri 2005). It can then be concluded that in this vertical stress σ_v range the effects of water content and dry density are negligible. This phenomenon can be explained as follows: The compression behavior mainly results from the compression of small pores inside soil aggregate (intra-aggregate pores) and the large pores between aggregates (inter-aggregate pores) (Ahmed *et al.* 1974). When the soil is in a relative low stress state, merely intra-aggregate pores are compressed, which occupy a small proportion, leading to a pretty slight decrease in void ratio.

However, when σ_v is larger than σ'_y, the variation of e would be highly dependent on water content and dry density. This is because when σ_v is large enough, void ratio e would decrease in terms of both large pores between soil aggregates and the aggregate and small pores inside soil aggregate (Wang *et al.* 2019). Since different water content and dry density would lead to substantial differences in soil fabric consisting of soil aggregates (see MIP results in Fig. 8 and 10 and SEM results in Figs. 9 and 11), appreciable water content and dry density dependency of e variation with σ_v can be expected.

It can be observed from Fig. 4(a) that for the specimens with same water content, when the dry density increases, the compression parameter λ characterizing the slope of the second part of the compression curve would decrease. This is because at same water content, with the increase of dry density, the quantity of large pores formed between soil aggregates decreases (see Figs. 8 and 9), leading to a decrease in compression parameter λ. When it comes to the effect of water content, as shown in Fig. 4(a), the increase of water content increases the compressibiliy parameter λ. This phenomenon can be attributed to the fact that the increasing water content increases the size of the silt clay aggregate and the number of large pores between them. In addition, the increasing water content favors the formation of clay matrix. Correspondingly, the amount of clay aggregates decreases. As reported by Delage *et al.* (2006), compared with clay aggregate, the clay matrix is easier to be compressed.

As for the influences of dry density and initial water content on the yield stress σ'_y, it is observed from Fig. 4(b) that both of them have significant influence on the σ'_y. This phenomenon is under expectation since the increase of the dry density decreases the compressibility parameter λ, the increase of water content increases the compressibility parameter λ, as described above. In Fig. 4(b), the variations of σ'_y with dry density and water content are observed to be opposite to the λ variation *w*ith both parameters. This can be attributed to the fact that σ'_y is determined from the intersection between the elastic compression slope and the plastic compression slope. Since the elastic compression parameter does not change with dry density and moisture content, the variation trends of yield stress σ'_y with dry density and initial water content would be similar to the variation trends of plastic compressibility parameter.

4.2 Influence of dry density and initial water content on the shear strength

As far as the water content effect on shear strength is concerned, the strength decreases with water content increasing (Fig. 5). This is because the shear behavior of compacted loess is closely related to soil structure (Wen *et al.* 2014). The SEM results (Fig. 11) show that when compacted at dry side of optimum moisture content (OMC), the soil microstructure is controlled by clay aggregate skeleton with silt grains coated on the surface, while when compacted at the wet side of OMC, the soil microstructure is controlled by clay matrixs. The pore-size distribution is plotted in Fig. 10. As can be observed, a bimodal distribution characterizes the dry side, while a tri-modal distribution characterizes the wet side. These features can be used to explain the variation of shear strength with water

content (see Fig. 5). On the dry side, the soil structure and aggregates govern the stiffness of soil, with the increase of water content, (silt-clay and clay) aggregates are gradually wetted and the aggregate grains become more and more disintegrated (Fig. 11). As a result, the deformation of soil structure which linked by clay cementations gives rise to a decrease of shear strength. Thus, on the wet side, the aggregates are destroyed as show in Fig. 11(b), 11(c) and the suction start to govern the soil stiffness, the suction monotonically decrease with increasing water content (Chang and Cheng 2018, Muñoz-Castelblanco *et al*. 2012), the decreasing of capillary suction involves a decreasing surface tension of the menisci water. Thus, the induced normal force between particles decreases, leading to the decrease of shear strength (Mancuso *et al.* 2002).

As far as the effect of dry density is concerned, the strength increased with dry density increasing (Fig. 5). This phenomenon can be explained as follows. As shown in Fig. 9, when dry density increases, the soil structure would become denser and correspondingly the contact area between soil particles increased, leading to an increase in shear strength.

5. Conclusions

In this study, a series of macro-level mechanical tests (one-dimensional compression tests and direct shear tests) and micro-level tests (SEM and MIP tests) are carried out on the compacted loess soil with various water contents and dry density. The following conclusions are drawn:

• The dry density and water content have a significant effect on compressibility parameters and shear strength. With the increasing of dry density, yield stress σ'_y, shear strength q, cohesion c and friction angle φ all show a steady growth, except for plastic parameter λ. On the contrary, with the increase of water content, yield stress σ'_y, shear strength q, cohesion c and friction angle φ all decrease to a certain extent except for plastic parameter λ. It is worth mentioning that neither dry density and water content have a significant effect on elastic parameter κ.

• The microstructures are sharply influenced by water content. For the specimens with the same dry density, if water content is smaller than the OMC, the sample is more prone to be bimodal structure. If water content is equal to OMC, the specimen would be trimodal structured, creating a new medium pores population of the clay matric pores due to partial clay developed structure. If water content is larger than OMC, a large portion of wet clayey friction is well-developed and it would transform a large number of large pores into medium pores, make a small portion of clay aggregate coat silt grains. In the end, a small amount of large pores would still exist.

• The microstructures are sharply influenced by dry density. For the specimens with the same water content, if dry density is relatively low, the structure is mainly dominated by inter-aggregate type with large pores, and it is very loose to deform and damage. By contrast, if dry density is relatively high, some proportion of aggregates would deform and a dense matrix microstructure would be built. The dense microstructure would be dominated by small pores and it contains a close arrangement of aggregates.

• A detailed explanation of the links among water content, dry density, structure and mechanical parameters is made. The mechanical behavior of compacted loess is closely related to its structure. For the specimens with lower dry density but higher water content, the large and medium pores in loess soil structure collapse and would be destroyed easier. Thus, the mechanical parameters would be significantly affected by water content and dry density. By contrast, for the specimens with higher dry density but lower water content, the large and medium pores in soil structure would vanish. As a result, the mechanical parameters are no obviously affected by water content and dry density.

Acknowledgments

Financial support comes from the the Shanxi Key Research and Development Program (No.2017DXM-SF-087).

References

Ahmed, S., Lovely C.W. and Diamond, S. (1974), "Pore sizes and strength of compacted clay", *J. Geotech. Eng. Div.*, **100**(GT4), 407-425. https://doi.org/10.1680/geot.1974.24.2.223.

Alshihabi, O., Shahrour, I. and Mieussens, C. (2002), "Chemo-mechanical coupling in saturated porous media: Elastic-plastic behaviour of homoionic expansive clays", *Int. J. Solids Struct.*, **10**(39), 2773-2806. https://doi.org/10.1016/S0020-7683(02)00151-8.

Assallay, A.M., Rogers, C.D.F. and Smalley, I.J. (1997), "Formation and collapse of metastable particle packings and open structures in loess deposits", *Eng. Geol.*, **48**(1-2), 101-115. https://doi.org/10.1016/S0013-7952(97)81916-3.

Casini, F., Vaunat, J. and Romero, E. (2012), "Consequences on water retention properties of double-porosity features in a compacted silt", *Acta Geotech.*, **7**(2), 139-150. https://doi.org/10.1007/s11440-012-0159-6.

Chang, C.C. and Cheng, D.H. (2018), "Predicting the soil water retention curve from the particle size distribution based on a pore space geometry containing slit-shaped spaces", *Hydrol. Earth Syst. Sci.*, **22**, 4621-4632. https://doi.org/10.5194/hess-22-4621-2018

Chen, B., Sun, D.A. and Jin, P. (2019), "Experimental study of the effect of microstructure on the permeability of saturated soft clays", *Geomech. Eng.*, **18**(1), 49-58. https://doi.org/10.12989/gae.2019.18.1.049.

Chen, R.P., Qi, S., Wang, H.L. and Cui, Y.J. (2019), "Microstructure and hydraulic properties of coarse grained subgrade soil used in high-speed railway at various compaction degrees", *J. Mater. Civ. Eng.*, **31**(12),04019301. https://doi/10.1061/(ASCE)MT.1943-5533.0002972.

Collins, K. and McGown, A. (1974), "The form and function of microfabric features in a variety of natural soils", *Géotechnique.*, **24**(2), 223-254. https://doi.org/10.1680/geot.1974.24.2.223.

Cui, Y.J. and Delage, P. (1996), "Yielding and plastic behaviour of an unsaturated compacted silt", *Géotechnique*, **46**(2), 291-311.

https://doi.org/10.1680/geot.1996.46.2.291.
Cuisinier, O. and Masrouri, F. (2005), "Hydromechanical behaviour of a compacted swelling soil over a wide suction range", *Eng. Geol.*, **81**, 204-212. https://doi.org/10.1016/j.enggeo.2005.06.008.
Delage. P., Marcial, D., Cui, Y.J. and Ruiz, X. (2006), "Ageing effects in a compacted bentonite: A microstructure approach", *Géotechnique.*, **56**, 291-304. https://doi.org/10.1680/geot.2006.56.5.291.
Derbyshire, E. and Mellors, T.W. (1988), "Geological and geotechnical characteristics of some loess and loessic soils from China and Britain: a comparison", *Eng. Geol.*, **25**(2), 135-175. https://doi.org/10.1016/0013-7952(88)90024-5.
Dijkstra, T.A., Smalley, I.J. and Rogers, C.D.F. (1995), "Particle packing in loess deposits and the problem of structure collapse and hydroconsolidation", *Eng. Geol.*, **40**, 49-64. https://doi.org/10.1016/0148-9062(96)81826-2.
Estabragh, A.R. and Javadi, A.A. (2015), "Effect of soil density and suction on the elastic and plastic parameters of unsaturated silty soil", *Int. J. Geomech.*, **15**(5), 1-12. https://doi.org/10.1061/(ASCE)GM.1943-5622.0000422.
Fredlund, D.J. and Rahardjo, H. (1993), *Soil Mechanics for Unsaturated Soils*, John Wiley & Sons, New York, U.S.A.
Haeri, M., Khosravi, A., Garakani, A.A. and Ghazizadeh, S. (2016), "Effffect of soil structure and disturbance on hydromechanical behavior of collapsible loessial soils", *Int. J. Geomech.*, **17**(1), 04016021-1-04016021-15. https://doi.org/10.1061/(ASCE)GM.1943-5622.0000656.
Hu, C.M., Wang, X.Y., Mei, Y., Yuan, Y.L. and Zhang, S.S. (2018), "Compaction techniques and construction parameters of loess as filling material", *Geomech. Eng.*, **15**(6), 1143-1151. https://doi.org/10.12989/gae.2018.15.6.1143.
Kim, D. and Kang, S.S. (2013), "Engineering properties of compacted loesses as construction materials", *KSCE. J. Civ. Eng.*, **17**(2),335-341. https://doi.org/10.1007/s12205-013-0872-1.
Kruse Gerard, A.M., Dijkstra, A.M. and Schokking, F. (2007), "Effect of soil structure on soil behaviour: illustrated with loess, glacially loaded clay and simulated flaster bedding examples", *Eng. Geol.*, **91**, 34-45. https://doi.org/10.1016/j.enggeo.2006.12.011.
Lloret, A., Villar, M. V., Sanchez, M., Gens, A., Pintado, X. and Alonso, E.E. (2003), "Mechanical behaviour of heavily compacted bentonite under high suction changes", *Géotechnique*, **53**(1), 27-40. https://doi.org/10.1680/geot.2003.53.1.27.
Mancuso, C., Vassallo, R. and Onofrio, A. (2002), "Small strain behavior of a silty sand in controlled-suction resonant column-torsional shear tests", *Can. Geotech. J.*, **31**(1), 22-31. https://doi.org/10.1139/t01-076.
Monroy, R., Zdravkovic, L. and Ridley, A. (2010), "Evolution of microstructure in compacted London clay during wetting and loading", *Géotechnique*, **60**(2), 105-119. https://doi.org/10.1680/geot.8.P.125.
Muñoz-Castelblanco, J.A., Pereira, J.M., Delage, P. and Cui, Y.J. (2012), "The water retention properties of a natural unsaturated loess from Northern France", *Géotechnique*, **62**(2), 95-106. https://doi.org/10.1680/geot.9.p.084.
Ng, CWW., Sadeghi, H., Hossen, S.B., Chiu, C.F., Alonso, E.E. and Baghbanrezvan, S. (2016), "Water retention and volumetric characteristics of intact and re-compacted loess", *Can. Geotech. J.*, **53**(8), 1258-1269. https://doi.org/10.1139/cgj-2015-0364.
Niu, G., Shao, L., Sun, D.A. and Guo, X. (2020), "A simplified directly determination of soil-water retention curve from pore size distribution", *Geomech. Eng.*, **20**(5), 411-420. https://doi.org/10.12989/gae.2020.20.5.411
Parviz, N., Shen, ZS., Yunus, M. and Zulqarnain, S. (2020), "Loess deposits in southern Tajikistan (Central Asia): Magnetic properties and paleoclimate", *Quarter. Geochronology.*, **60**(101114), 1-12. https://doi.org/10.1016/j.quageo.2020.101114.
Penumadu. D. and Dean. J. (2000), "Compressibility effect in evaluating the pore-size distribution of kaolin clay using mercury intrusion porosimetry", *Can. Geotech. J.*, **37**(2), 393-405. https://doi.org/10.1139/t99-121.
Rogers, C.D.F., Dijkstra, T.A. and Smalley, l.J. (1994), "Particle packing from an earth-science viewpoint", *Earth Sci. Rev.*, **36**(1-2), 59-82. https://doi.org/10.1016/0013-7952(94)90001-9.
Romero, E., Della Vecchia, G. and Jommi, C. (2011), "An insight into the water retention properties of compacted clayey soils", *Géotechnique*, **61**(4), 313-328. https://doi.org/10.1007/s11709-011-0108-8.
Wang, J.D., Li, P., Ma, Y. and Vanapalli, S.K. (2019), "Evolution of pore-size distribution of intact loess and remolded loess due to consolidation", *J. Soils. Sediments*, **19**(3), 1226-1238. https://doi.org/10.1007/s11368-018-2136-7.
Wen, B.P. and Yan, Y.J. (2014), "Influence of structure on shear characteristics of the unsaturated loess in Lanzhou, China", *Eng. Geol.*, **168**, 46-58. https://doi.org/10.1016/j.enggeo.2013.10.023.
Yates, K., Fenton, C.H. and Bell, D.H. (2018), "A review of the geotechnical characteristics of loess and loess-derived soils from Canterbury, South Island, New Zealand", *Eng. Geol.*, **236**, 11-21. https://doi.org/10.1016/j.enggeo.2017.08.001.
Zhang, F., Ye, W.M., Chen, Y.G., Chen, B. and Cui, Y.J. (2016), "Influences of salt solution concentration and vertical stress during saturation on the volume change behavior of compacted GMZ01 bentonite", *Eng. Geol.*, **207**, 48-55. https://doi.org/10.1016/j.enggeo.2016.04.010.

IC